II

Spatiotemporal Dynamics of Synchronous Activity across Multiple Areas of the Visual Cortex in the Alert Monkey

Charles M. Gray and Baldwin Goodell

Introduction

The variability of neuronal activity in the brain is enigmatic. In mammals, complex neural interactions, occurring in parallel across widely distributed networks, enable an astounding repertoire of flexible behavior. One might assume that such analytical and computational power, to borrow a phrase from information technology, would be associated with highly reliable and robust neural activity patterns that are tightly correlated with behavior. Yet, when measured from just about any location in the Telencephalon, neuronal activity appears noisy, unreliable and often weakly linked to behavior and events in the external world. Detecting the relationships that do exist typically requires extensive behavioral training of the subject and repeated measurements to "average out the noise.". Perhaps this situation is to be expected, given that neurons are intrinsically nonlinear and much of their activity depends on patterns of input from tens of thousands of weak, probabilistic and plastic synapses. It does, however, beg the question of how such variable and dynamic neuronal activity can

underlie the impressive perceptual, motor and cognitive capabilities of mammals. Perhaps we are simply unable to measure the activity of enough neurons simultaneously to identify the networks that are engaged in particular cognitive processes. Or, perhaps more likely, we have yet to identify the neural dynamics that underlie specific cognitive functions. One can't help but be impressed with how much we don't understand.

The realization that the brain is a nonlinear dynamical system (Freeman and Skarda, 1985; Kelso, 1995; Friston, 2000; Izhikevich, 2007; Izhikevich and Edelman, 2008) may account for some of the difficulty. The brain, and the cortex in particular, is generally regarded as a parallel distributed system, composed of enormous numbers of highly nonlinear and adaptable neurons, that are organized into hierarchical networks with multiple, nested levels of feedback. Even simple systems having these properties are notorious for their emergent and unpredictable behavior, and the brain is certainly the epitome of such a system. Thus, it should come as no surprise that the activity of individual neurons, embedded within distributed neural networks, often shows little or no relation to experimental manipulations and displays inexplicable variability. Unlike explanatory theories in physics and chemistry, however, the development of a systems level theory of distributed neural processing is still at an early stage (Buzsáki, 2006). We therefore lack a clear search image for identifying large-scale, emergent patterns of neural activity that are robustly linked to behavior. This often leads to a heuristic approach and a focus on problems that are technically feasible. This problem is analogous to that faced by the drunk who is looking for his lost keys under the streetlight because that's where the light is.

This is not to discount or ignore the many impressive advances in systems neuroscience, but rather highlight the unique challenges posed by understanding distributed neural processing. Perhaps the field is at a developmental stage similar to what Kuhn (1962) referred to as a 'pre-paradigm period,'" in which competing schools of thought use different methods and are guided by differing theories and presuppositions. If one accepts this premise, it implies that cognitive/systems neuroscience is largely an empirical enterprise, which raises the question of what aspects of neural activity should be measured and analyzed to gain the greatest insights. A case can be made that a useful approach is to cast a broad net, ground one's observations in sound physiological principles, and characterize phenomena closely related to behavior.

In this chapter, we present preliminary results from experiments that have attempted to take this approach at face value. Our broad net has been to initiate the design and development of instruments that enable the recording of unit activity and local field potentials from large numbers of chronically implanted,

and independently movable, microelectrodes. We have borrowed design concepts from other successful efforts (Wilson and McNaughton, 1993; deCharms et al., 1999; Hoffman and McNaughton, 2002; Csicsvari et al., 2003; Miller and Wilson, 2008) and developed new devices for long-term recordings of distributed neural activity in awake/behaving monkeys. Our grounding in neurophysiology, and the behavioral correlates of mesoscopic brain states, stems from our own work (Gray et al., 1986, 1989; Gray and McCormick, 1996; Azouz and Gray, 2000; Maldonado et al., 2000), and that of many others (Freeman and Skarda, 1985; Bressler 1995; Singer, 1999; Usrey and Reid, 1999; Freeman, 2000; Varela et al., 2001; Buzsáki and Draguhn, 2004; Fries 2005; Buzsáki, 2006), and focuses on the properties, underlying neural mechanisms, and behavioral correlates of distributed patterns of synchronous neuronal activity.

We infer, on the basis of a large body of existing evidence, that spatially distributed patterns of synchronous activity play a fundamental role in cognitive brain function and that extensive characterization of these phenomena is needed. Our justification follows two lines of reasoning. At the cellular level, synchronous synaptic activity is known to be highly effective at driving postsynaptic responses (Alonso et al., 1996; Azouz and Gray, 2000, 2003) and plays a key role in regulating activity dependent synaptic plasticity (Markram et al., 1997; Bi and Poo, 1998). At the network level, distributed patterns of synchronous activity are robust, prevalent, and well correlated with sensory stimulation and cognitive aspects of behavior (for reviews see Gray, 1994; Singer and Gray, 1995; Bressler, 1995; Singer, 1999, 2009; Usrey and Reid, 1999; Buzsáki and Draguhn, 2004; Buzsáki, 2006; Fries, 2009, and more recent studies by Langheim et al., 2006; Buschman and Miller, 2007; Saalmann et al., 2007; Zhang et al., 2008; Pesaran et al., 2008; Lubenov and Siapas, 2009; Gregoriou et al., 2009). In spite of this extensive work, however, we believe that the characterization of distributed activity patterns and their relationships to cognition and behavior, and the development of new theory, is still in its infancy. This situation is somewhat analogous to the state of astronomy, circa 1920, before the discovery of galaxies lying beyond the Milky Way (Ferris, 1997). New instruments, in the form of large telescopes utilizing spectral analysis, confirmed the existence of distant galaxies and an expanding universe. This led to a wave of experimentation and theory development that continues unabated to this day.

With this context, we describe the results of our initial measurement and characterization of the spatiotemporal dynamics of the local field potential recorded from several areas of the visual cortex in an alert macaque monkey that is freely viewing a dynamic natural scene. Our findings indicate that perceptual

and cognitive processes involve large-scale, distributed patterns of synchronization that occur within and between multiple cortical areas. These patterns of correlated activity are transient, non-stationary, occur in multiple frequency bands, and reflect the time course of sensory and behavioral events.

Methods

We performed unit and local field potential recordings in a female macaque monkey, using a semi-chronically implanted array of sixty independently movable microelectrodes. Prior to recording, the animal was implanted with a post for fixation of the head, a scleral search coil for monitoring eye position, and a custom, hermetically-sealed recording chamber to enable mounting of the microdrive (Gray et al., 2007). The chamber was centered over area V4 in the left hemisphere. The monkey was trained to visually fixate a central target, to permit the mapping of cellular receptive fields, and to freely scan brief presentations of static natural scenes and movies.

The Chamber and Microdrive

The recording chamber system incorporates a replaceable Silastic membrane that provides a water-tight seal and an effective barrier to infection (see Gray et al., 2007, for details). The microdrive houses sixty linear actuators and contact with the microelectrodes (Tungsten-in-glass, Alpha Omega, Inc.) is established through a printed circuit board. The inter-electrode spacing is 1.2 mm and each actuator enables 6 mm of bi-directional electrode travel. The microdrive is 15 mm in diameter, 32 mm in height and, when mounted within the chamber, the bottom surface of the drive lies flush against the Silastic membrane.

Figure 11.1 shows the fully loaded microdrive with fifty-seven of the sixty electrodes advanced for testing impedance and the mechanical integrity of each actuator. (Three of the actuators failed during the loading process.) Prior to mounting the microdrive in the chamber, the guide holes in the bottom of the drive were back-filled with ophthalmic antibiotic ointment, and the bottom surface of the drive was covered with a thin layer of sterile, molten bone wax (Swadlow et al., 2004). These steps insure sterility and minimize the back flow of fluid into the actuators. Once these steps were completed, the microdrive was mounted within the chamber, fixed in place with a retaining cap, and the assembly reinforced with a supplemental layer of acrylic cement that extended up to the lower flange on the retaining cap.

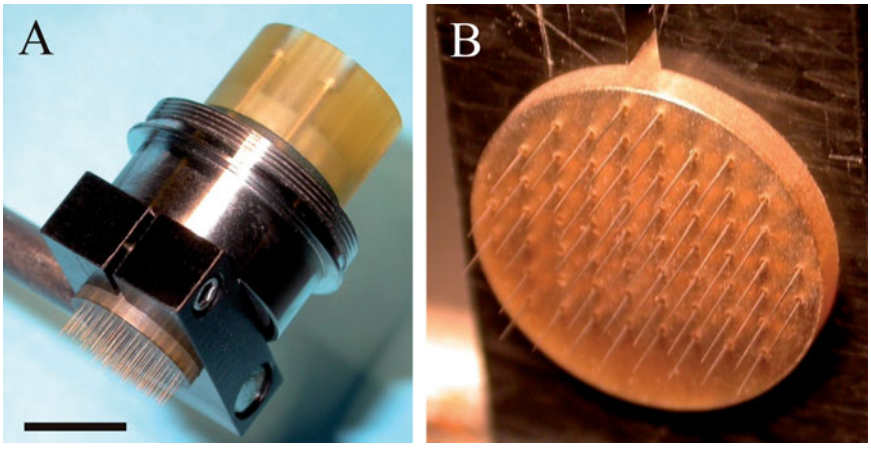

FIGURE 11.1 Photographs of the semichronic microdrive prior to its implantation. A) Tilted view of the microdrive mounted in a holder. All 57 electrodes are advanced. B) Close up view of the electrode tips. Scale bar in A is 6 mm.

Electrophysiological Recording

Once the microdrive was mounted within the chamber, the microelectrodes were gradually advanced into the cortex over a period of five to seven days, and recordings of unit activity and local field potentials were performed five days a week for a total of twenty-five days. Each day the monkey viewed a color movie on a computer monitor placed at a distance of 57 cm. Data sets were collected during periods of one to three minutes of continuous viewing at the beginning of each session and after a set of electrodes (typically five to ten) had been incrementally advanced to isolate activity at new sites.

At the end of this first experiment, a second microdrive, containing thirty-two independently movable microelectrodes (20 mm travel, 2 mm interelectrode spacing), was implanted at the same location in the right hemisphere. A similar series of measurements were made using this drive. These data are still being analyzed. Following the second experiment, the animal was euthanized, perfused transcardially with fixative and the brain removed and photographed with the overlying skull and implant intact. This enabled us to accurately identify the recording locations of each of the electrodes in both hemispheres relative to the sulcul landmarks. The reconstructed recording locations in the left hemisphere are shown in Figure 11.2. The recording array spanned at least four separate areas of the visual cortex, including areas V1, V2, V4 and 7a.

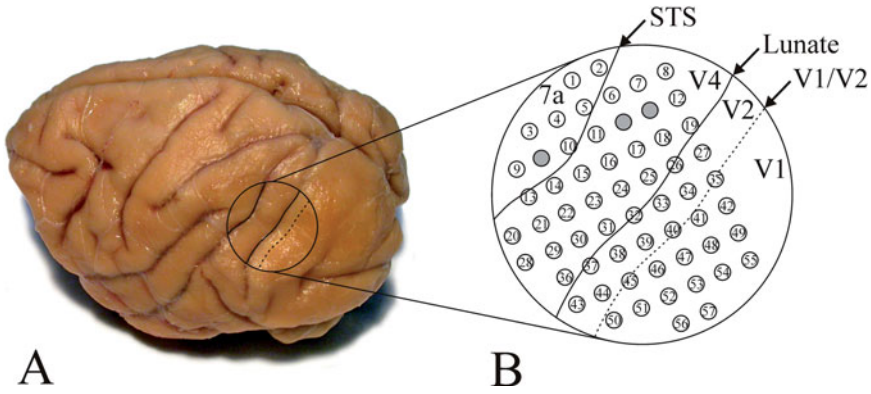

FIGURE 11.2 Reconstruction of the recording locations from the 60-channel array
A) Photograph of the left hemisphere of the monkey's brain. The boundary of the recording chamber is shown by the circle. B) Expanded schematic of the recording locations of each of the 57 electrodes. The sulci and visual cortical areas are labeled. An estimate of the V1/V2 boundary is shown by the dashed line. Bad channels are shown by the gray filled circles. STS – Superior Temporal Sulcus.

Data Analysis

The aim of the data analysis was to measure and characterize the spatiotemporal patterns of correlated local field potential (LFP) fluctuations measured across the array. For this, we employed a sliding window cross-correlation analysis, previously developed by us to characterize synchronous activity in area 17 of the cat (Gray et al., 1992). Each signal from the electrode array was bandpass filtered (10-100 Hz) and down-sampled to a rate of 1 kHz. A 2 sec segment of the filtered signals from fifty-seven electrodes is shown in Figure 11.3. This example, taken from ~1 minute of data while the monkey was visually scanning a movie, illustrates the highly dynamic nature of the spatial and temporal properties of the LFP. Higher numbered channels, located within V1, and possibly V2 (see Figure 11.2B), exhibit pronounced episodes of synchronized gamma-band (30–60 Hz) activity. Lower and intermediate numbered channels exhibit signals in the beta-band (12–30 Hz) having varying degrees of correlation, and also appear to be independent of the activity occurring in areas V1 and V2.

To evaluate these spatiotemporal interactions with high resolution, we calculated a time-lagged cross-correlogram (1 ms resolution) within a sliding window (110 ms duration, 20 ms step size) spanning a range of ±20 ms time lags for all possible channel combinations (n=1596 chn pairs) in the array. Figure 11.4 illustrates the analysis method. A short segment of the LFP data taken from two channels in the array (blue and green) is shown in A. Part B shows

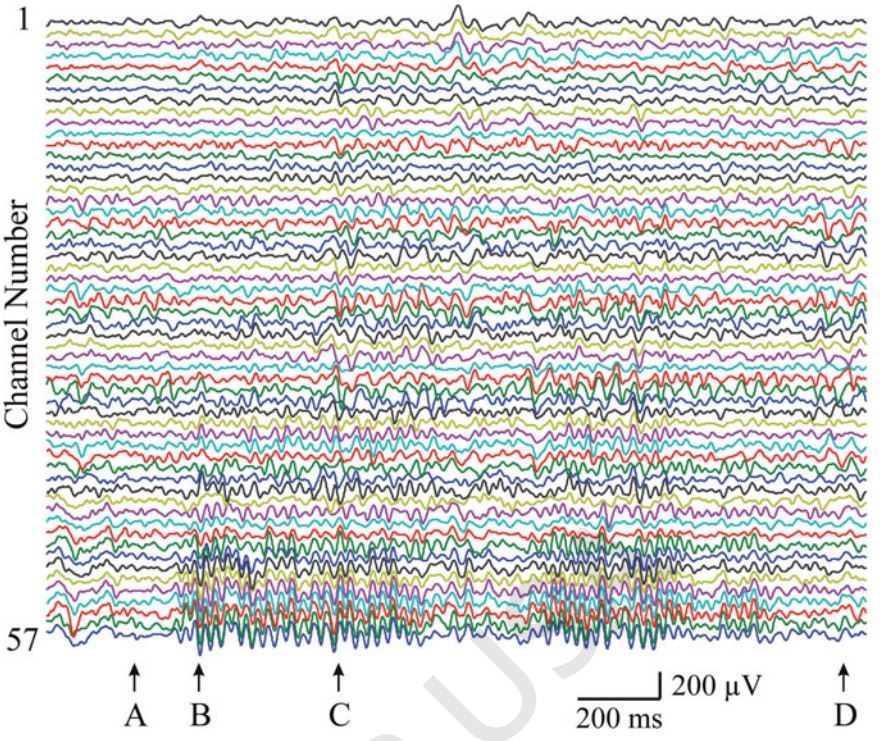

FIGURE 11.3 LFP signals from 57 channels of the array during a 2 second period while the monkey freely viewed a movie. The signals were band pass filtered (10-100 Hz). The arrows labeled A-D mark time points that correspond to the correlation maps in Figure 7.

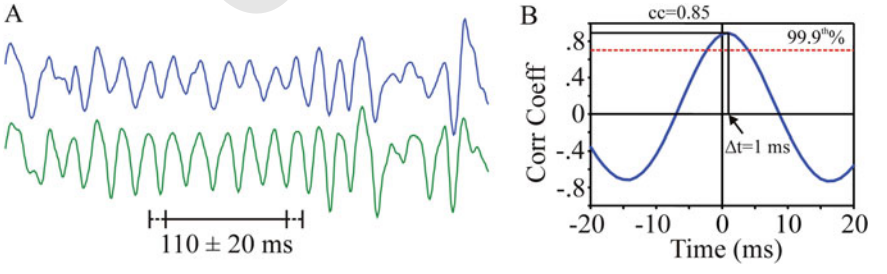

FIGURE 11.4 Sliding window correlation analysis A) Short segment of LFP signals (bandpass filtered 10-100 Hz) from two adjacent channels. The scale bar indicates the duration of the sampling window and the dashed lines indicate the range of time lags and the magnitude of the time step of the windowed analysis. B) Cross correlogram computed from the data segment shown by the scale bar in A. The red dashed line indicates the 99.9% confidence limit. The magnitude and time lag of the correlogram peak are indicated by the horizontal and vertical lines, respectively.

the cross-correlogram computed from the segment shown below the traces in A. For each step in the windowed analysis, we determined the magnitude and time-lag (i.e. phase) of the positive correlation peak closest to time 0. In this example, the positive peak had a value of 0.85 at a delay (Δt) of +1 ms. To test for the significance of this value, we computed a set of 1,000 surrogate correlation coefficients at 0 ms time-lag by independent and random sampling of the window locations in the two channels across the entire recording session. This yielded a Gaussian distribution of correlation coefficients with a maximum centered near 0. The positive value in this distribution, at which 99.9% of the data fell below, served as the threshold for statistical significance. This value, indicated by the dashed red line in B, served as the significance threshold for all time steps of the windowed analysis across the data set for this channel pair. An identical calculation was performed for each channel pair across the array, thereby providing a separate significance threshold for each pair of LFP signals. (The resulting threshold values fell within a narrow range across channels.)

An example of the results of this analysis for two different channel pairs (electrodes 29–55, 55–57), is shown in Figure 11.5. Channel 29 sampled activity from area V4 and channels 55 and 57 were located within area V1 and separated by approximately 2.2 mm (see Figure 11.2). The traces in A (chns 55, 57) and B (chns 29, 55) show the LFP signals (red, blue) and the peak correlation coefficient (black) as a function of time for a 2 sec epoch of the recording. The scale for the correlation coefficients is shown at left, and the threshold for significance ($P<.001$) is indicated by the black dashed line. The two signals in V1 (A) were highly correlated, with correlation coefficients often rising above the significance threshold. In contrast, the signals on channels 29 and 55 (B) appeared to be largely independent of one another, having only one time step where the correlation coefficient exceeded the significance threshold. The phase differences between the two pairs of signals (i.e. time-lag in ms) are shown in part C. The blue and green traces correspond to the channel pairs in A (55–57) and B (29–55), respectively. The signals recorded in V1 (55-57) tend to remain close to 0 ms time-lag, particularly during the periods where the correlation coefficients exceed the significance threshold. The second pair of signals (29–55), recorded in V4 and V1, display a broad range of time-lags indicative of two independent signals.

We applied this analysis to the same channel pairs for the entire 1-minute duration of the session. Figure 11.6 shows the distributions of significant correlation coefficients (A,D), their corresponding time-lags (B,E), and the durations of temporally continuous periods of significant correlation (C,F). The data from the V1 channel pair (55–57) and the V4/V1 channel pair (29–55) are shown in the top and bottom rows, respectively. For the V1 pair, significant

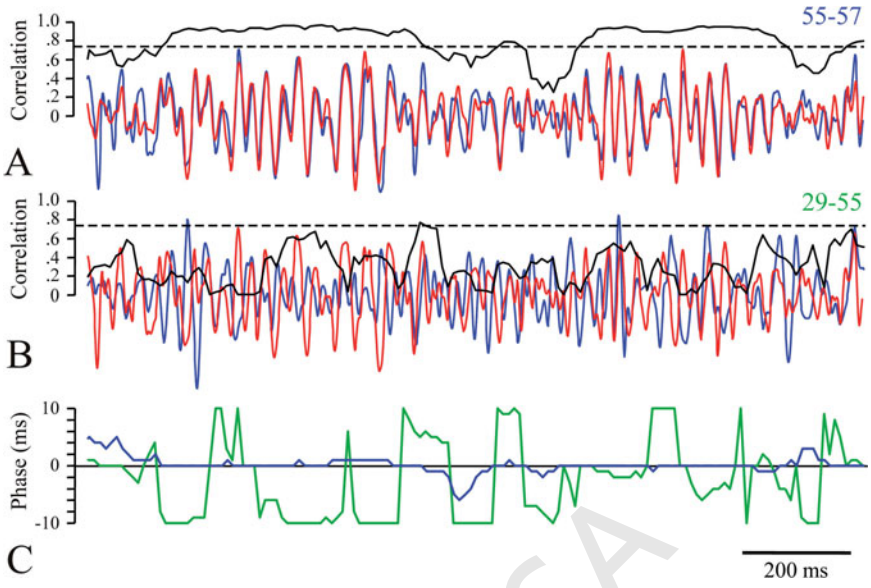

FIGURE 11.5 Sliding window correlation analysis The plots in A and B show pairs of LFP signals (red, blue) and their corresponding time-dependent correlation coefficients (black) for a 2 sec segment of data taken from channels 55–57 (A) and 29–55 (B). The 99.9% confidence limit is marked by the dashed lines in each plot. The plot in C shows the corresponding time-lags of the correlation peaks as a function of time. The blue and green traces were computed from the signal pairs in A and B, respectively.

correlations were robust and prevalent. The mean value of the correlation coefficients that exceeded the significance threshold was 0.85, and the two signals were significantly correlated 58% of the time. The distribution of time-lags for these coefficients was centered at 0 (mean=0.1 ms) and displayed very little variation (stdev=1.06 ms). In addition, when the two signals became correlated, the duration of these events had a median value of 160 ms and a maximum of ~1 sec.

In contrast, the correlations between the V4/V1 pair were much weaker and very sparse. The mean significant correlation coefficient was 0.76, and the signals were significantly correlated only 1% of the time. The distribution of time-lags was essentially random. There was no clear peak in the distribution and the standard deviation was 14.6 ms. Moreover, the distribution of correlation durations had a median value of 20 ms, suggesting that nearly all the significant correlation events were due to chance crossings of the significance threshold at some random phase. These data showed no indication of

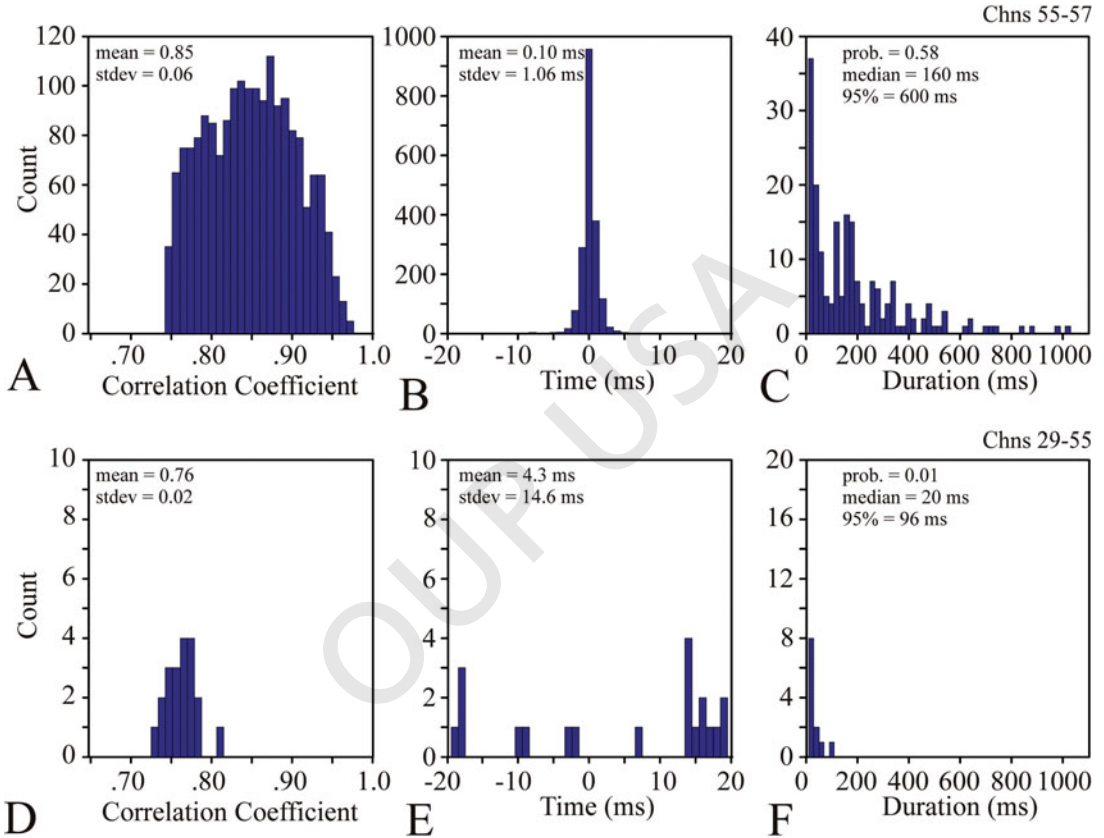

FIGURE 11.6 Properties of the time-dependent correlations computed from the two channel pairs illustrated in Figure 11.5. A,D) Distribution of significant correlation coefficients ($p<.001$). B,E) Distribution of the corresponding time-lags. C,F) Distribution of the duration of continuous periods of significant correlation.

systematic temporal correlation and suggest that this pair of V4 and V1 signals are independent.

In order to characterize the spatiotemporal patterns of synchronization, we considered it important to identify, and then exclude, correlations in the data that were likely to have occurred by chance, and thus not reflect true cortico-cortical interactions. Evidence for these types of spurious correlations was apparent in the V4/V1 signal pair shown in Figure 11.6. We therefore applied the same analysis to all channel pairs in the data set (n=1596) and plotted the results as a function of the spatial separation between the electrode pairs (data not shown). *(Note that the separations were calculated from the electrode spacing in the array and did not take into account the depths of the electrodes or the cortical separation distance based on the curvature and sulcal patterns in the cortex.)* These data revealed that the magnitude, duration and probability of significant correlation decreased with distance, while the variance in the time-lag of the correlations increased with distance. We used these data, along with inspection of the individual time-lag histograms, to select thresholds for exclusion of channel pairs and individual correlation coefficients, whose values were indicative of chance correlations. A channel pair was excluded from the analysis when at least one of the following conditions was met: (1) the mean significant correlation coefficient was < 0.7 (*this led to the exclusion of only one channel pair*), (2) the standard deviation of the time lag distribution was > 9 ms, (3) the median duration of the correlation events was < 60 ms, and (4) the percentage of time the signals were significantly correlated was < 1%. Even when these criteria were applied, we continued to find correlations in the remaining signal pairs in which the distribution of time-lags was centered at, or near, 0 ms, but had some large values lying outside the central distribution. We suspected that these events also represented spurious correlations and applied the additional threshold to exclude correlation coefficients in which the absolute value of the time lag was > 6 ms.

Results

Having applied these thresholds, we were able to characterize the spatiotemporal properties of synchronous activity across the array. An example of this is shown in Figure 11.7. The four panels show separate snapshots of the spatial distribution of significant correlation coefficients for the four corresponding epochs labeled A–D in Figure 11.3. There are at least three distinct correlated networks that are apparent in these examples. During the period marked by A, the distribution of correlations is sparse, comparatively weak and relatively

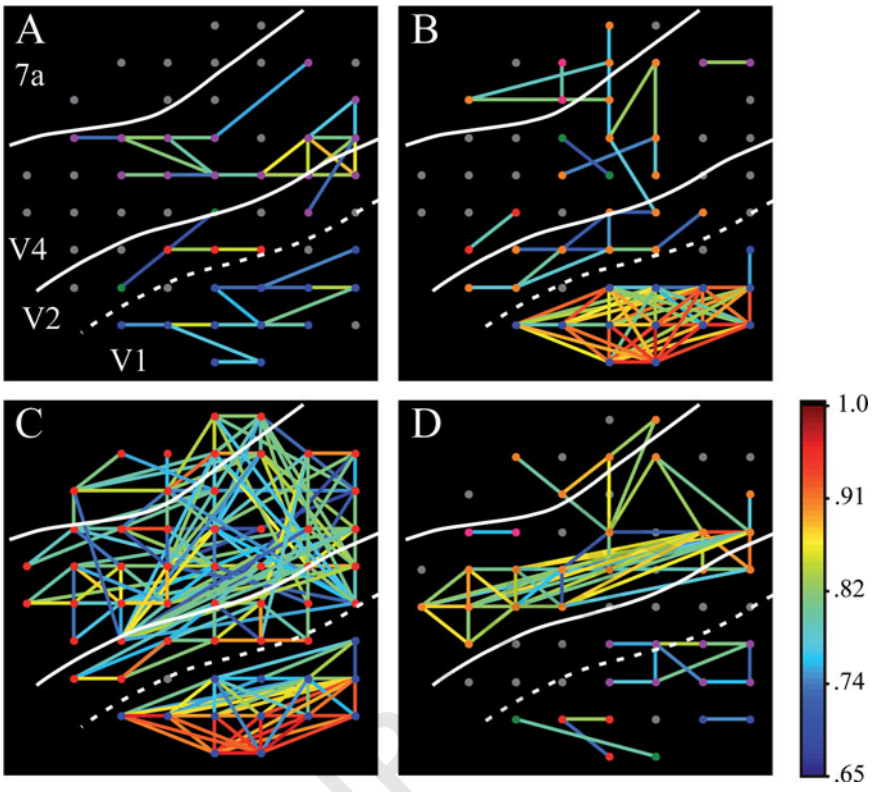

FIGURE 11.7 Static maps of all thresholded and statistically significant ($p<.001$) pair-wise correlations of LFP signals across the array. The maps labeled A-D were computed from the data centered on the four time points marked by the arrows in Figure 11.3. The white solid and dashed lines correspond to the areal boundaries illustrated in Figure 11.2.

devoid of spatial structure. This occurs during a period where the LFP signals show minimal temporal structure. A sharp transition occurs in B, where a well-defined network appears in area V1 with strong correlations and high amplitude oscillations in the gamma frequency band (see B in Figure. 11.3). The remaining correlations anterior to V1 are sparse, weaker, and show little temporal structure. A second transition occurs in panel C, where two independent networks are clearly visible. This is associated with a maintained gamma oscillation in V1 and the onset of synchronous oscillations in the high beta range anterior to V1. This second, anterior network is still relatively sparse compared to that occurring in V1. A third network is apparent during the period illustrated by D in Figures 11.3 and 11.7. This network was limited to the central portion of the array corresponding to area V4 and was characterized

by synchronous oscillations in the low beta frequency range, while relatively little activity was apparent in V1 and anterior to the STS.

These data demonstrate a striking dynamic character to the spatio-temporal patterns of synchronous activity in the visual cortex. In the span of a few hundred milliseconds, multiple, synchronous networks of activity can form, collapse and reform, and with each new instance their structure can vary in its spatial distribution, spectral content, and degree of interaction across multiple cortical areas. While revealing, many additional questions are raised by these findings. One would like to know the properties of the visual stimuli that evoke these patterns, their relationship to eye movements, the extent to which cognitive factors such as attention contribute to their structure, and the spatial organization of the networks, such as the size of the networks and the extent to which they show coupling between multiple cortical areas.

In order to explore one aspect of these questions, we implemented some simple calculations, borrowed from graph theory and the analysis of small world networks (Watts and Strogatz, 1998; Sporns, 2002; Bassett and Bullmore, 2006; Sakkalis et al., 2006), to characterize the number, size, spatial extent, and connection density of the synchronous networks. Each recording location (i.e., signal) in the array is considered to be a "node." A "network" consists of a minimum of two signals that are significantly correlated for a minimum duration of 60 ms (i.e., three time steps in the moving window analysis) and this interaction represents an edge or "connection" between a pair of nodes. Unlike the graphs discussed in Sporns (2002), indirect connections between nodes are not considered in our analysis. The size of a network is determined by the number of connections it contains, and multiple networks can coexist within each time step of the analysis so long as there are no connections between them. The length of a connection is defined as the Euclidian distance between locations in the array (in millimeters), and as mentioned earlier does not take into account the depth of the recording nor the curvature of the cortex. From these conventions, "connection density" is defined as the ratio of the observed number of connections at each time step relative to the total number of possible connections (i.e. n=1596).

The results of these calculations are shown in Figure 11.8 and represent the properties of all the detected networks from approximately one minute of recording time. The connection density for all observed networks is relatively sparse and has a median value of .05 (A). Thus, on average, only 5% of the possible pairwise correlations are present across the array. The number of coexisting networks ranges from 1–13 and has a median value of 6 (B). Hence, it is uncommon for only a single network to be observed at any given time, but large numbers of coexisting networks are also very rare. The median size of the

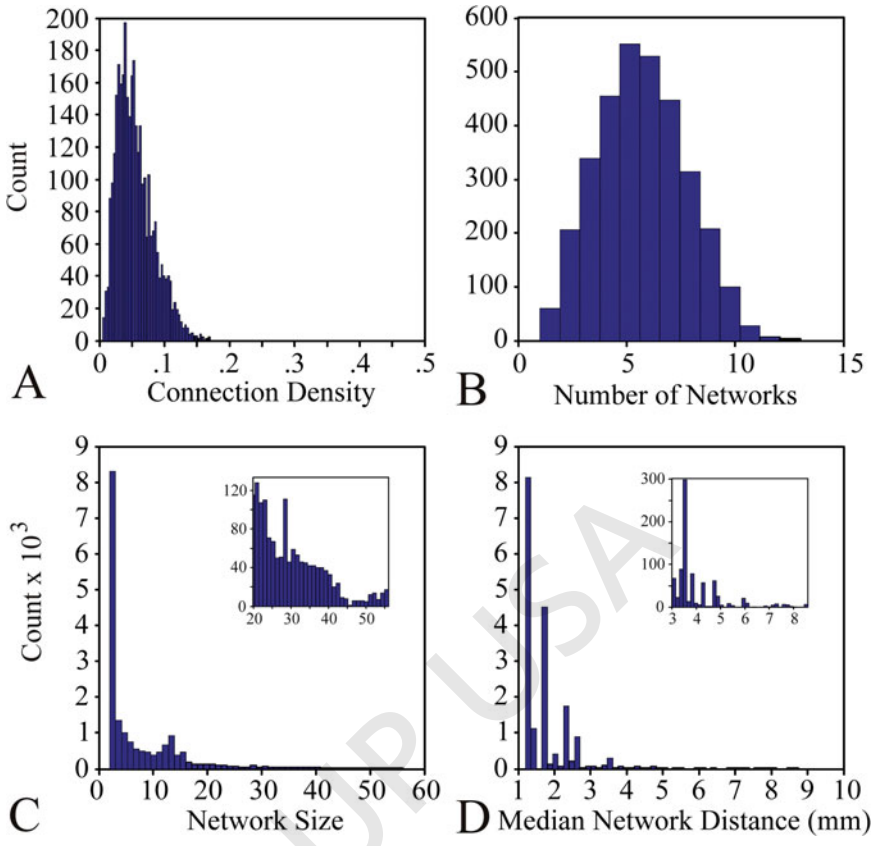

FIGURE 11.8 Histograms of connection density (A), number of networks (B), network size (C) and median network distance (D) computed from the entire 1-minute of data sampled from the 60-channel array while the monkey freely viewed a movie.

observed networks is 4, indicating that networks of only a few connections are by far the most common (C), but larger networks are also prevalent (see inset in C). We also characterized the spatial dimensions of the synchronous networks by calculating the median length (in millimeters) among the connections in all observed networks (D). As expected, these data demonstrate that most networks are composed of connected nodes that are adjacent or nearby to one another. Occasionally, however, networks of larger spatial scale are present (see inset in D). Finally, scatter plots of these variables revealed that as connection density across the array increased the number of networks decreased, and the maximum network size increased (data not shown). Thus increases in connectivity across the array were associated with fewer numbers of networks having larger sizes.

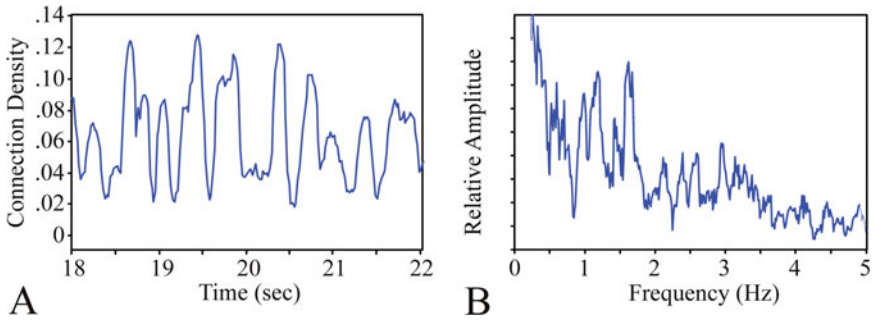

FIGURE 11.9 Time dependent properties of the synchronous networks A. Connection density as a function of time for a 2-second segment of data. B. Power spectrum of the connection density versus time for the entire 1-minute period of data collection.

In order to gain some additional insight into the temporal organization of these networks, we performed some additional analyses of the time-dependent changes in these network parameters. Because both network size and the number of networks were closely correlated with connection density, we restricted our analysis to the latter variable. Figure 11.9 shows the time-dependent changes in connection density across the array. The plot in A shows a 2-second segment of connection density as a function of time. Large, semi-periodic fluctuations are apparent with time scales on the order of ~200-500 ms. The power spectrum of connection density for the entire 1-minute recording session (B) supports this observation. Multiple frequency components are present in the data and prominent peaks occur at approximately 1, 1.5, 2.5 and 3 Hz. Thus, there is a striking dynamic organization to the time-dependent changes in synchronous cortical networks. Large changes in the number of visual cortical networks, their connection density, and their size occur rapidly, on the order of hundreds of milliseconds, as the monkey freely scans a dynamic natural scene.

These findings of course raise the question of how the network organization varies with respect to the properties of the visual scene and the animal's saccadic eye movements. These questions are unfortunately beyond the scope of our initial investigation. In these early recordings, our ability to acquire the eye position signals during the free-viewing task was constrained by some technical factors. We were thus unable to evaluate the network dynamics with respect to eye movements and the image properties in the movie. In the second series of experiments, utilizing a thirty-two-channel array in the opposite hemisphere (see Methods), we solved the former problem and are thus able to provide some limited insight into the relation between network organization and

eye movements. The placement of this second array was very similar to that of the first. The electrodes sampled activity from areas V1, V2, V4 and 7a. We collected data from the monkey over a period of eight weeks, and on each recording day the animal freely viewed a movie for several sessions, each lasting several minutes.

The analysis of these data is still in progress, but visual inspection of the raw data has revealed some interesting relationships between saccadic eye movements and the occurrence and properties of synchronous networks. A typical example of these data is shown in Figure 11.10. This plot shows the vertical and horizontal components of the monkey's eye movements (V,H) along with the broadband (0.5 Hz – 10 kHz) signal recorded from electrodes in V1, near the V1/V2 border, for a 2-second period. The onset of visual fixation, at each new target chosen by the animal, is marked by a vertical line. A striking property of these signals is the occurrence of brief synchronous gamma-band oscillations that follow the onset of some visual fixations and

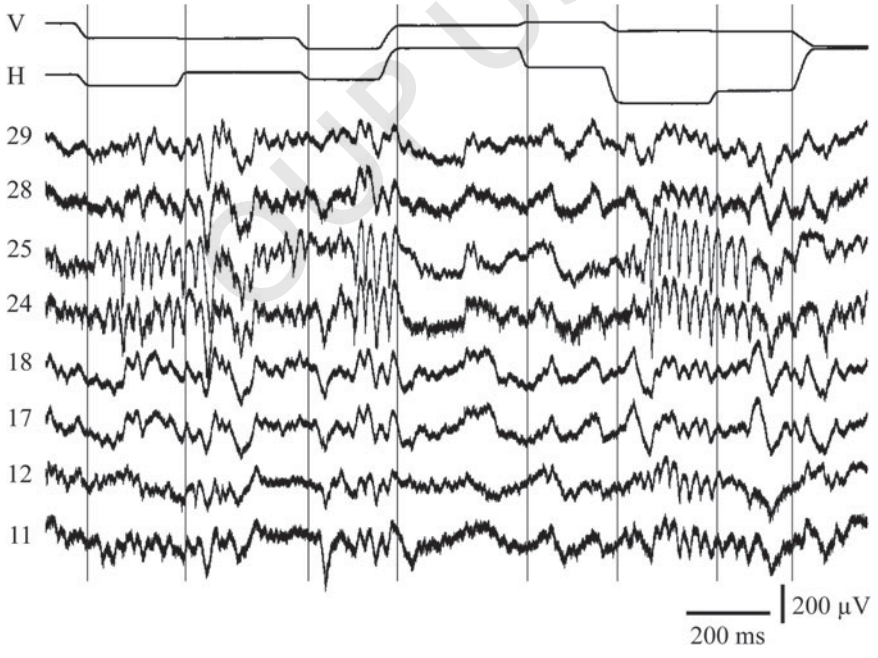

FIGURE 11.10 A short segment of raw data sampled from the 32-channel array in the right hemisphere while the monkey freely viewed a movie. The upper two traces show the vertical and horizontal components of the eye movements. The remaining traces show the broadband signal (1 Hz – 10 kHz) sampled from 8 of the electrodes located in area V1 near the V1/V2 border.

not others. The latency, duration, amplitude and spatial distribution of these bursts also vary across fixations. In some instances the synchronous activity spans multiple fixations or can be truncated by the evoked response following the onset of a new fixation. While these data are preliminary, and we have not characterized the image properties in relation to the animal's eye movements, we can be certain that the image projected on the retina changes markedly from one visual fixation to the next. Thus, it is reasonable to assume that the fluctuations in network organization described above are strongly dependent on the properties of the visual images.

Discussion

Using a newly developed instrument, and time-dependent correlation analysis, to measure correlated local field potential fluctuations from multiple visual cortical areas simultaneously, we find striking stimulus-dependent, dynamic patterns of synchrony that occur within and between several areas of the visual cortex. These findings are consistent with a number of theoretical predictions concerning the dynamics of cortico-cortical interactions (Gray, 1999; Singer, 1999, 2009; Friston, 2000; Fries, 2005; Buzsáki, 2006). They demonstrate that multiple, independent synchronous assemblies can form and dissipate rapidly, follow complex spatiotemporal trajectories, and vary in their spatial distribution and spectral composition over a wide range of frequencies. The synchronous networks tend to remain confined to cortical area boundaries, but also encompass multiple areas in many instances. These initial data suggest that gamma-band networks are formed largely in V1, possibly V2, and that they follow the onset of fixation at a latency ranging from 50-100ms, a result supported by a recent study in V1 of free-viewing monkeys (Maldonado et al., 2008).

These results are also cause for optimism. While not reported here, we have found from ongoing measurements in V1, as well as prefrontal and posterior parietal cortex (Salazar et al., 2008), that it is possible to measure multi- and single-unit activity from fixed recording locations for periods lasting one to two weeks or longer. These data suggest that the chronic recordings are not damaging the cortical tissue, as might be expected if the brain were moving relative to the recording array that is rigidly mounted on the skull. Moreover, an advantage of the method is that once adequate data has been sampled, or if activity has deteriorated over time, new signals (units and field potentials) can be sampled by advancing one or all of the electrodes. In this way it is possible to collect extensive data sets that not only span multiple cortical areas, but also

sample activity across cortical layers, into the depths of sulci, and from subcortical nuclei.

The data presented here are clearly preliminary, however, and many questions remain to be addressed. Detailed analysis needs to be performed to establish the relationship between saccadic eye movements, the properties of the visual image during each period of fixation, and the spatiotemporal organization of the synchronous networks. In our second set of recordings, described in Figure 11.10, we have found many instances in which evoked responses follow saccades at short latency. These common events are readily detected by our method and are likely to account for some fraction of the synchronous networks we have measured. Other robust networks, such as those detected in V1, follow the onset of fixation and occasionally span saccadic eye movements suggesting a potential mechanism for temporal integration across successive visual fixations. In retinotopically organized areas we should expect to find transient synchronous networks that reflect the features in the retinal image or the salience of objects (Gray, 1999). Whereas in nonretinotopic areas the patterns may be indicative of the behavioral significance of the images, the intention to make an eye movement to a particular location or target, or the attention directed to some aspect of the visual scene.

Analytically, there is much room for improvement as well. We chose to measure correlations in the time domain because this enabled us to use smaller temporal windows than conventional time-frequency analysis (Mitra and Pesaran, 1999; Grinsted et al., 2004) and avoid the need for repeated observations or signal averaging (Ding et al., 2000) which would have eliminated the real-time nature of the measurements. This prevented us from characterizing the frequency distribution of the interactions and forced us to express phase in units of milliseconds. Perhaps other more powerful methods, such as Empirical Mode Decomposition (Liang et al., 2005) or Frequency Flows Analysis (Rudrauf et al., 2006) could provide a more effective basis for analysis of these data.

Finally, our findings, and the feasibility of the recording methods, may open up a broad new area of investigation of distributed processing in the mammalian brain. The chamber system and microdrive array can easily be expanded to sample activity from much larger areas of the brain. New devices can extend the travel of the electrodes, decrease the inter-electrode spacing to enable higher sampling density, and incorporate additional instruments for electrical stimulation, drug delivery or the use of an optical neural interface (Aravanis et al., 2007; Han et al., 2009). Currently, we are developing a system to enable high-density microelectrode recording from an entire hemisphere in macaque monkeys (Goodell and Gray, 2008). Implementation of such a device will no doubt present many challenges. It will also provide unprecedented

access to the brain to permit the analysis of distributed processes on a scale comparable to functional imaging methods, but with much higher spatial and temporal resolution. Data from these and related instruments will likely lead to the development of new analytical methods to observe and characterize distributed patterns of neural activity that have been beyond the scope of our current methods. Perhaps then we will metaphorically see beyond our own galaxy and observe the large scale dynamics of the brain.

REFERENCES

Alonso, J.M., Usrey, W.M., Reid, R.C. (1996) Precisely correlated firing in cells of the lateral geniculate nucleus. *Nature, 383*, 815–819.

Aravanis, A., Wang, L.P., Zhang, F., Meltzer, L., Mogri, M., Schneider, M.B., Deisseroth, K. (2007) An optical neural interface: *in vivo* control of rodent motor cortex with integrated fiberoptic and optogenetic technology. *Journal of Neural Engineering, 4,* S143–S156.

Azouz, R., Gray, C.M. (2000) Dynamic spike threshold reveals a mechanism for synaptic coincidence detection in cortical neurons *invVivo*. Proceedings of the Nationall Academy of Science, 97(14), 8110–8115.

Azouz, R., Gray, C.M. (2003) Adaptive coincidence detection and dynamic gain control in visual cortical neurons *in vivo. Neuron, 37,* 513–523.

Bassett, D.S., Bullmore, E. (2006) Small-world brain networks. *Neuroscientist, 12(6),* 512–523.

Bi, G.Q., Poo, M.M. (1998) Synaptic modifications in cultured hippocampal neurons: dependence on spike timing, synaptic strength, and postsynaptic cell type. *J of Neuroscience, 18,* 10464–10472.

Bressler, S.L. (1995) Large-scale cortical networks and cognition. *Brain Res Rev, 20,* 288–304.

Buschman, T.J. and Miller, E.K. (2007) Top-down versus bottom-up control of attention in the prefrontal and posterior parietal cortices. *Science, 315,* 1860-1862.

Buzsáki G. (2006) Rhythms of the Brain. Oxford University Press.

Buzsáki, G. and Draguhn, A. (2004) Neuronal oscillations in cortical networks. *Science, 304,* 1926–1929.

Csicsvari, J., Henze, D.A., Jamieson, B., Harris, K.D., Sirota, A., Wise, K.D., Buzsáki, G. (2003) Massively parallel recording of unit and local field potentials with silicon-based electrodes. *J of Neurophysiology, 90,* 1314–1323.

DeCharms, R.C., Blake, D.T., Merzenich, M.M. (1999) A multielectrode implant device for the cerebral cortex. *J. Neurosci Meth., 93,* :27–35.

Ding, M., Bressler, S.L., Yang, W., Liang, H. (2000) Spectral analysis of cortical event-related potentials by adaptive multivariate autoregressive modeling: Model order, stability and consistency. *Biol Cybern, 83,* 35–45.

Ferris T. (1997) The whole shebang. New York: Touchstone.

Freeman, W.J. (2000) Mesoscopic neurodynamics: from neuron to brain. *J Physiol Paris, 94,* 303–322.

Freeman, W.J. and Skarda, C.A. (1985) Spatial EEG patterns, non-linear dynamics and perception: the neo-Sherringtonian view. *Brain Res, 357,* 147–175.

Fries, P. (2005) A mechanism for cognitive dynamics: neuronal communication through neuronal coherence. *Trends Cogn Sci, 9,* 474–480.

Fries, P. (2009) Neuronal gamma-band synchronization as a fundamental process in cortical computation. *Annu Rev Neurosci, 32,* 209–224.

Friston, K.J. (2000) The labile brain. I. Neuronal transients and nonlinear coupling. *Philos Trans R Soc Lond B Biol Sci, 355,* 215–236.

Goodell, A.B. and Gray, C.M. (2008) A large-scale, distributed recording system for semi-chronic monitoring of cortical and sub-cortical neuronal activity in alert monkeys. *Soc Neurosci Abs,* 101.7.

Gray, C.M. (1994) *Synchronous oscillations in neuronal systems: mechanisms and functions. J. of Computational Neuroscience, 1,* 11–38.

Gray, C.M. (1999) The temporal correlation hypothesis of visual feature integration: Still alive and well. Neuron, 24, 31–47.

Gray, C.M., Engel, A.K, Koenig, P., Singer, W. (1992) Synchronization of oscillatory neuronal responses in cat striate cortex: Temporal properties. *Visual Neuroscience, 8,* 337–347.

Gray, C.M., Freeman, W.J., Skinner, J.E. (1986) Chemical dependencies of learning in the olfactory bulb: acquisition of the transient spatial pattern change depends on norepinephrine. *Behavioral Neuroscience, 100(4),* 585–596.

Gray CM, Goodell AB, Lear AT. (2007) A Multi-Channel Micromanipulator and Chamber System for Recording Multi-Neuronal Activity in Alert, Non-Human Primates. *J. Neurophysiol., 98,* 527–536.

Gray. C.M., Koenig, P., Engel, A.K., Singer, W. (1989) Stimulus-specific neuronal oscillations in cat visual cortex exhibit inter-columnar synchronization which reflects global stimulus properties. *Nature, 338,* 334–337.

Gray, C.M., McCormick, D.A. (1996) Chattering cells: Superficial pyramidal neurons contributing to the generation of synchronous oscillations in visual ortex. *Science, 274,* 109–113.

Gregoriou, G.G., Gotts, S.J., Zhou, H., Desimone, R. (2009) High-frequency, long-range coupling between prefrontal and visual cortex during attention. *Science, 324,* 1207–1210.

Grinsted, A., Moore, J.C., Jevrejeva, S. (2004) Application of the cross wavelet transform and wavelet coherence to geophysical time series. *Nonlinear Processes in Geophysics, 11,* 561–566.

Han, X., Qian, X., Bernstein, J.G., Zhou, H.H., Franzesi, G.T., Stern, P., Bronson, R.T., Graybiel, A.M., Desimone, R., Boyden, E.S. (2009) Millisecond-timescale optical control of neural dynamics in the nonhuman primate brain. *Neuron, 62,* 191–198.

Hoffman, K.L. and McNaughton, B.L. (2002) Coordinated reactivation of distributed memory traces in primate neocortex. *Science, 297,* 2070–2073.

Izhikevich, E.M. (2007) *Dynamical systems in neuroscience: The geometry of excitability and bursting*. Cambridge: MIT Press.

Izhikevich, E.M. and Edelman, G.M. (2008) Large-scale model of mammalian thalamo-cortical systems. *Proceedings of the National Academy of Science*, 105, 3593–3598.

Kelso, J. (1995) *Dynamic patterns: The self-organization of brain and behavior*. Cambridge: MIT Press.

Kuhn, T.S. (1962) *The structure of scientific revolutions*. Chicago: University of Chicago Press.

Langheim, F.J., Leuthold, A.C., Georgopoulos, A.P. (2006) Synchronous dynamic brain networks revealed by magnetoencephalography. *ProcEedings of the National Academy of Science, 103,* 455–459.

Liang, H., Bressler, S.L., Buffalo, E.A., Desimone, R., Fries, P. (2005) Empirical mode decomposition of field potentials from macaque V4 in visual spatial attention. *Biol Cybern., 92,* 380–392.

Lubenov, E.V. and Siapas, A.G. (2009) Hippocampal theta oscillations are travelling waves. *Nature, 459,* :534–539.

Maldonado, P., Babul, C., Singer, W., Rodriguez, E., Berger, D., Gruen, S. (2008) Synchronization of neuronal responses in primary visual cortex of monkeys viewing natural images. *J of Neurophysiology 100,* 1523–1532.

Maldonado, P.E., Friedman-Hill. S.R., Gray, C.M. (2000) Dynamics of striate cortical activity in the alert macaque: II. Fast time scale synchronization. *Cerebral Cortex, 10,* 1117–1131.

Markram, H., Lubke, J., Frotscher, M., Sakmann, B. (1997) Regulation of synaptic efficacy by coincidence of postsynaptic APs and EPSPs. *Science, 275*, 213–215.

Miller, E.K. and Wilson, M.A. (2008) All my circuits: using multiple electrodes to understand functioning neural networks. Neuron, 60, 483–488.

Mitra, P.P. and Pesaran, B. (1999) Analysis of dynamics brain imaging data. *Biophys J, 76*, 691–708.

Pesaran, B., Nelson, M.J., Andersen, R.A. (2008) Free choice activates a decision circuit between frontal and parietal cortex. *Nature, 453,* 406–409.

Rudrauf, D., Douiri, A., Kovach, C., Lachaux, J.P., Cosmelli, D., Chavez, M., Adam, C., Renault. B., Martinerie, J., Le Van Quyen. M. (2006) Frequency flows and the time-frequency dynamics of multivariate phase synchronization in brain signals. *Neuroimage, 31*, 209–227.

Sakkalis, V., Oikonomou, T., Pachou, E., Tollis. I., Micheloyannis. S., Zervakis M. (2006) Time-significant wavelet coherence for the evaluation of schizophrenic brain activity using a graph theory approach. *Conf Proc IEEE Eng Med Biol Soc, 1,* 4265–4268.

Saalmann, Y.B., Pigarev, I.N., Vidyasagar, T.R. (2007) Neural mechanisms of visual attention: how top-down feedback highlights relevant locations. *Science, 316,* 1612–1615.

Salazar, R.F., Bressler, S, Richter, C., Gray, C.M. (2008) Fronto-parietal coherence is task and rule specific. *Soc Neurosci Abs*, 418, 9.

Singer, W. (1999) Neuronal synchrony: a versatile code for the definition of relations? *Neuron, 24*, 49–65.

Singer, W. (2009) Distributed processing and temporal codes in neuronal networks. *Cogn Neurodyn., Jun 28*. [Epub ahead of print]

Singer, W. and Gray, C.M. (1995) Visual feature integration and the temporal correlation hypothesis. *Ann. Rev. Neurosci, 18,* 555–586.

Sporns, O. (2002) Graph theory methods for the analysis of neural connectivity patterns. In Kotter, R. (Ed.), *Neuroscience Databases. A Practical Guide*. Boston: Kluwer; 171–186.

Swadlow, H.A., Bereshpolova, Y., Bezdudnaya, T., Cano, M., Stoelzel, C.R. (2004) A multi-channel, implantable microdrive system for use with sharp, ultra-fine "Reitboeck" microelectrodes. *J. of Neurophysiology, 93*, 2959–2965.

Usrey, W.M., and Reid, R.C. (1999) *Synchronous activity in the visual system. Annual Review of Physiology, 61*, 435-56.

Varela, F., Lachaux, J.P., Rodriguez, E., Martinerie. J. (2001) The brainweb: phase synchronization and large-scale integration. *Nat. Rev. Neurosci, 2,* 229–239.

Watts, D.J. and Strogatz, S.H. (1998) Collective dynamics of"small-world" networks. *Nature, 393,* 440–442.

Wilson, M.A. and McNaughton, B.L. (1993) Dynamics of the hippocampal ensemble code for space. *Science, 261*, 1055–1058.

Zhang, Y., Wang, X., Bressler, S.L., Chen, Y., Ding, M. (2008) Prestimulus cortical activity is correlated with speed of visuomotor processing. *J Cogn Neurosci, 20,* 1915–1925.